

# Constraints on the Clustering, Biasing and Redshift Distribution of Radio Sources

M. Magliocchetti <sup>1</sup>, S.J. Maddox <sup>1</sup>, O. Lahav <sup>1</sup>, J.V. Wall <sup>2</sup>

<sup>1</sup>*Institute of Astronomy, Madingley Road, Cambridge CB3 0HA*

<sup>2</sup>*Royal Greenwich Observatory, Madingley Road, Cambridge CB3 0EZ*

14 July 2021

## ABSTRACT

We discuss how different theoretical predictions for the variance  $\sigma^2$  of the counts-in-cells distribution of radio sources can be matched to measurements from the FIRST survey at different flux limits. The predictions are given by the integration of models for the angular correlation function  $w(\theta)$  for three different functional forms of the redshift distribution  $N(z)$ , different spatial correlation functions that match the observed present day shape and by different evolutions of the bias  $b(z)$  with redshift. We also consider the two cases of open and flat Universes. Although the predicted  $w(\theta)$  show substantial differences due to differences in the  $N(z)$ 's, these differences are not significant compared to the uncertainties in the current observations. It turns out that, independent of the geometry of the universe and the flux limit, the best fit is provided by models with constant biasing at all times, although the difference between models with epoch-independent bias and models with bias that evolves linearly with redshift is not very large. All models with strong evolution of bias with epoch are ruled out as they grossly overestimate the amplitude of the variance over the whole range of angular scales sampled by the counts-in-cells analysis. As a further step we directly calculated  $w_{obs}(\theta)$  at 3mJy from the catalogue and matched it with our models for the angular correlation function in the hypothesis that the clustering signal comes from two different populations, namely AGN-powered sources and starbursting galaxies. The results are consistent with a scenario for hierarchical clustering where the fainter starbursting galaxies trace the mass at all epochs, while the brighter AGN's are strongly biased, with  $b(z)$  evolving linearly with redshift, as suggested by some theories of galaxy formation and evolution.

**Key words:** galaxies: clustering - radio galaxies - cosmology: theory - large-scale structure

## 1 INTRODUCTION

During the past few years there has been an increasing interest in how galaxies trace mass and specifically in the issue of a biasing factor evolving with redshift (e.g. Fry, 1996; Bagla, 1997; Matarrese et al., 1997; Moscardini et al., 1997; Tegmark & Peebles, 1998). This has received added impetus after Steidel et al. (1996, 1997) reported evidence for a strong concentration of galaxies at  $z \sim 3$  (Lyman-Break Galaxies), which would imply a value of  $b \sim 6$  at those redshifts.

Radio objects can be detected up to very significant cosmological distances ( $z \sim 4$ ) and therefore provide information on large scale structure at rather early epochs when the main growth of structures occurred. Even though evidence of clus-

tering in radio catalogues was detected in early wide-area surveys (Seldner & Peebles, 1981; Shaver & Pierre, 1989; Kooiman et al., 1995; Sicotte, 1995; Loan, Wall & Lahav, 1997), the FIRST survey (Becker et al., 1995) is the first one in which the angular clustering of radio sources down to the mJy level is detected with high signal to noise ratio (Cress et al., 1997; Magliocchetti et al., 1998). Unfortunately the relation between angular measurements and spatial quantities is strongly dependent on the radio source redshift distribution  $N(z)$ , which becomes more and more uncertain as the flux threshold is lowered. Dunlop and Peacock (DP, 1990) provided models of epoch-dependent luminosity functions for radio sources to make estimates of  $N(z)$  that work well for bright sources, but these predictions drastically diverge at faint fluxes. One of the main uncertainties at such low flux densities is given by the presence and relative amplitude of a

low-redshift spike due to a population of starbursting galaxies (e.g. Windhorst et al., 1985) now believed to constitute a majority of sources at mJy levels (see Wall, 1994 for an overview).

The knowledge of a well assessed functional form for the redshift distribution of radio sources  $N(z)$  has become of crucial importance in the last decade for both radio-astronomy and cosmology. In the former case this would provide tests for radio-source unification and luminosity evolution models (Wall & Jackson, 1997), while in the latter case it would allow conversion of angular clustering measurements to spatial clustering estimates that can be used to constrain structure formation models.

We present here a theoretical approach able to put constraints on both the functional form of  $N(z)$  at fluxes  $F \leq 10\text{mJy}$  and the clustering properties of radio objects. We pay particular attention to the evolution of bias, i.e. the way radio galaxies trace the mass distribution. We begin by assuming that the spatial correlation function of mass is determined by the linear growth of mass fluctuations. This is a reasonable assumption because the mean redshift of radio sources in the survey ( $\bar{z} \sim 1$  as opposed to  $\bar{z} \sim 0.1$  obtained for optical and infrared surveys), and so the angular scales that we consider correspond to physical scales where the linear theory still holds. The clustering of radio galaxies is then related to mass via three different models for the evolution of bias with redshift, each one related to a reasonable model for galaxy evolution, as taken from Matarrese et al., 1997 and Moscardini et al., 1997. We then predict the angular two-point correlation function  $w(\theta)$  for three models of  $N(z)$  that span the range realistic distributions for faint radio objects. We obtain the correlation function using both flat and open geometry.

In section 2 we introduce the different models for  $N(z)$  used in the projection analysis, while section 3 describes the calculation of the theoretical predictions for  $w(\theta)$ ; the predictions for each model are then presented in section 4. In section 5 we move to the analysis of the variance and we show the results obtained for the measurements of the  $\sigma^2$  of the distribution of sources in the FIRST survey at flux limits up to 10 mJy. The data are compared with our predictions from different models of  $w(\theta)$  in section 6. Section 7 presents our results on the interpretation of clustering and bias under the assumption that radio sources are formed by two different populations. Section 8 summarises our conclusions.

## 2 THE REDSHIFT DISTRIBUTION $N(z)$

To test the stability of the predicted angular correlation function given for different functional forms of the redshift distribution  $N(z)$ , we use the Dunlop & Peacock (DP, 1990) models of epoch-dependent space density for radio sources. These models used Maximum Entropy analysis to determine polynomial approximations to the luminosity function and its evolution with redshift; the approach incorporated the then-available identification and redshift data for complete samples from radio surveys at several frequencies.

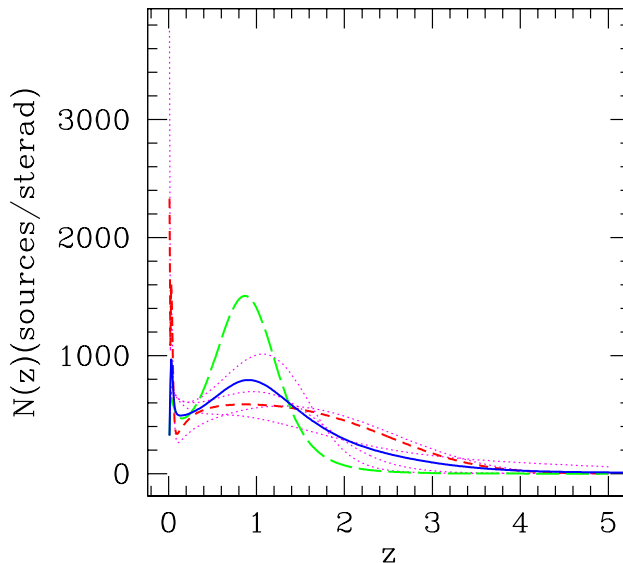


**Figure 1.** Redshift distribution  $N(z)$  for the radio source population at 1.4 GHz at a flux limit of 3 mJy. The dotted and dashed curves represent the 6 models (1-4, 6-7) taken from Dunlop & Peacock (1990); the solid curve is the average. Model 5 is omitted as it shows a totally unrealistic sharp and dominant feature at  $z = 4$

Figures 1 and 2 show, for flux limits of 3 and 10 mJy respectively, models 1-4 and 6-7 taken from DP (dotted-dashed lines) and their average (solid line). The discrepancies amongst different models become increasingly significant as the flux threshold is lowered, mirroring the lack of any information on radio objects at faint fluxes. We have chosen three models which span the range of reasonable  $N(z)$ ; two representing the extremes, and one intermediate.

The first model we adopted is DP's 7 (called hereafter N3), indicated by Peacock (private communication) as the best model, which predicts  $N(z)$  for pure luminosity evolution. This is illustrated in figures 1 and 2 by the short-dashed line, and is characterised by a low-redshift component which becomes more dominant at fainter fluxes, and by a broad and shallow maximum for  $z \gtrsim 0.5$ . The low- $z$  spike could be interpreted as modelling the starburst-galaxy population which appears at these faint fluxes.

The second model considered in our analysis, DP's 3, (called hereafter N2) is represented in figures 1 and 2 by the long-dashed line; it has a narrow and prominent bump around  $z \sim 1$  and no low-redshift spike.

As an intermediate model N1 we chose the average of DP's 1-4, 6-7 for it shows both the low-redshift component and the  $z \sim 1$  bump, but neither feature is too dominant. This is plotted as the solid line in Figures 1 and 2.

## 3 PREDICTING THE ANGULAR CORRELATION FUNCTION

The standard way of relating the angular two-point correlation function  $w_{radio}(\theta)$  to the spatial two-point correlation function  $\xi_{radio}(r, z)$  is by means of the relativistic Limber

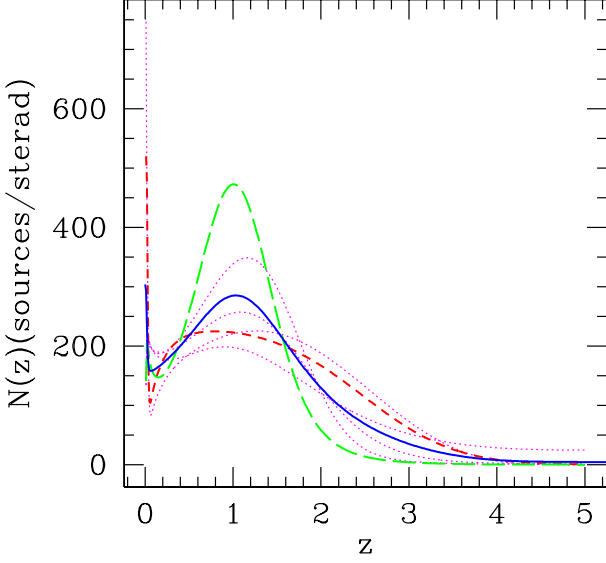


**Figure 2.** Redshift distribution  $N(z)$  for the radio source population at 1.4 GHz at 10 mJy. The dotted and dashed curves represent the 6 models (1-4, 6-7) taken from Dunlop & Peacock (1990); the solid curve is the average.

equation (Peebles, 1980):

$$w_{radio}(\theta) = 2 \frac{\int_0^\infty \int_0^\infty F^{-2}(x)x^4\Phi^2(x)\xi_{radio}(r,z)dx du}{\left[\int_0^\infty F^{-1}(x)x^2\Phi(x)dx\right]^2}, \quad (1)$$

where  $x$  is the comoving coordinate,  $F(x)$  gives the correction for curvature, and the selection function  $\Phi(x)$  is determined by the  $N(z)$ ,

$$\mathcal{N} = \int_0^\infty \Phi(x)F^{-1}(x)x^2 dx = \frac{1}{\Omega_s} \int_0^\infty N(z)dz, \quad (2)$$

in which  $\mathcal{N}$  is the mean surface density on a surface of solid angle  $\Omega_s$  and  $N(z)$  is the number of objects in the given survey within the shell  $(z, z + dz)$ .

The physical separation between two sources separated by an angle  $\theta$  is given (in the small angle approximation) by:

$$r \simeq \frac{1}{(1+z)} \left( \frac{u^2}{F^2} + x^2\theta^2 \right)^{1/2}. \quad (3)$$

The comoving coordinate  $x$  and the correction factor  $F(x)$  are different for different geometries; for a Universe with generic density parameter  $\Omega_0$  and cosmological constant  $\Lambda = 0$  (see e.g. Treyer & Lahav, 1996):

$$x = \frac{2c}{H_0} \left[ \frac{\Omega_0 z - (\Omega_0 - 2)(1 - \sqrt{1 + \Omega_0 z})}{\Omega_0^2(1+z)} \right] \quad (4)$$

and

$$F(x) = \left[ 1 + \left( \frac{H_0 x}{c} \right)^2 (\Omega_0 - 1) \right]^{1/2}. \quad (5)$$

This leads, with equation (2), to the following expression for

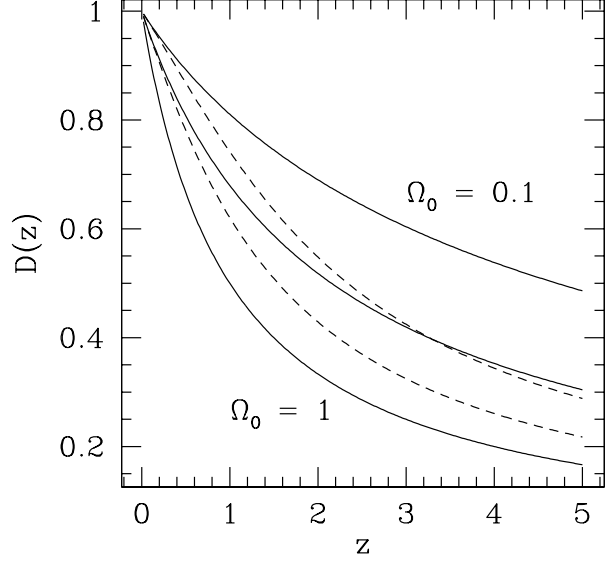


**Figure 3.** The linear-theory density growth  $D(z)$  scaled to unity at the present time for  $\Omega_0 = 1$ ,  $\Omega_0 = 0.3$  and  $\Omega_0 = 0.1$ . The solid lines represent open models ( $\Lambda = 0$ ) while the dashed lines are for flat models ( $\Lambda + \Omega_0 = 1$ ).

the angular correlation function:

$$w_{radio}(\theta) = 2 \frac{H_0 \Omega_0^2}{c} \frac{\int_0^\infty N^2(z)/P(\Omega_0, z)dz \int_0^\infty \xi_{radio}(r, z)du}{\left[\int_0^\infty N(z)dz\right]^2}, \quad (6)$$

where  $P(\Omega_0, z)$  is given by

$$P(\Omega_0, z) = \frac{4(\Omega_0 - 1)[(1 + \Omega_0 z)^{1/2} - 1] + \Omega_0^2(1 - z) + 2\Omega_0 z}{(1+z)^2(1 + \Omega_0 z)^{1/2}}, \quad (7)$$

and  $u$  is defined by (3).

In the case of a cosmological constant  $\Lambda \neq 0$  with  $\Omega_0 + \Lambda = 1$  (flat space), we have  $F(x) = 1$  and:

$$x = \frac{c}{H_0} \Omega_0^{-1/2} \int_0^z \frac{dz}{[(1+z)^3 + \Omega_0^{-1} - 1]^{1/2}}, \quad (8)$$

(see Peebles, 1984; Treyer & Lahav, 1996) so that the expression for  $w(\theta)$  assumes the form

$$w_{radio}(\theta) = 2 \frac{H_0}{c} \Omega_0^{1/2} \frac{\int_0^\infty N^2(z)Q(\Omega_0, z)dz \int_0^\infty \xi_{radio}(r, z)du}{\left[\int_0^\infty N(z)dz\right]^2}. \quad (9)$$

with

$$Q(\Omega_0, z) = [(1+z)^3 + \Omega_0^{-1} - 1]^{1/2} \quad (10)$$

To take into account the evolution of clustering with epoch, we express the correlation function  $\xi_{radio}(r, z)$  as:

$$\xi_{radio}(r, z) = \xi_{mass}(r)D^2(z)b^2(z), \quad (11)$$

We have chosen the present-day  $\xi_{mass}(r)$  to have a shape which matches the observed  $\xi_{gal}$  from local optical galaxy surveys (eg. APM, LCRS, etc.) and a normalization which matches the 4-year COBE data (Bunn & White 1997). On large scales we use the linear-theory prediction from the

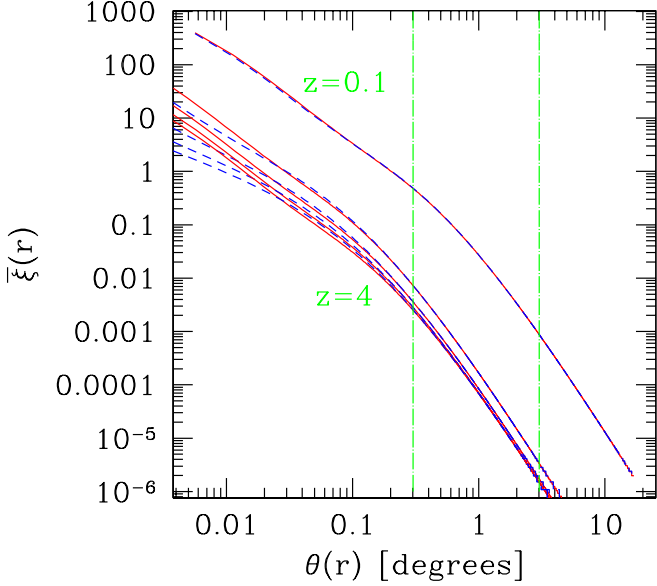


**Figure 4.** Integrated correlation function  $\bar{\xi}(r, z)$  as a function of the angular scale  $\theta$  in the case  $\Omega_0 = 1$  at redshift  $z = 0.1, 1, 2, 3, 4$ . Solid lines represent the predictions for growth of clustering under linear theory on the assumption of a  $\xi_{mass}(r)$  as described in the text, while the dashed lines take into account the effects of non-linear evolution. The two vertical lines bracket the range  $0.3^\circ \leq \theta \leq 3^\circ$  provided by the observations.

power spectrum  $P(k)$  of Bond & Efstathiou (1984). On small scales the linear prediction under-estimates the true amplitude, and so we extrapolated with a power-law of slope  $-1.7$ , as observed from the APM correlation function (Maddox et al., 1990). For  $\Gamma = 0.2$  the extrapolation is used for  $r \leq r_0^{gal} = 5.4\text{Mpc}$ . For other values of  $\Gamma$  we have re-scaled  $\xi$  so that  $\xi_1(r) \propto \xi_2(r\Gamma/2)$ . In each case we use the 4 year COBE data to fix the normalization in terms of mass fluctuations  $\sigma_8^{mass}$ .

$D(z)$  is the linear-theory density growth-rate whose generic expression is given by Peebles (1980) and Lahav et al. (1991);  $D(z) = (1+z)^{-1}$  for an Einstein-de Sitter Universe

$$f(z) \equiv \frac{d \ln(D(z))}{d \ln(a)} \quad (12)$$

with  $a = (1+z)^{-1}$  and  $f(z) \simeq R^{0.6}$ , where

$$R(z, \Omega_0, \Lambda) = \Omega_0(1+z)^3 [\Omega_0(1+z)^3 - (\Omega_0 + \Lambda - 1)(1+z)^2 + \Lambda]^{-1} \quad (13)$$

Figure 3 shows the behaviour of  $D(z)$  for a range of  $\Omega_0$  and  $\Lambda$ . Our choice to consider only the case for growth of clustering under linear theory is extensively discussed in Magliocchetti et al., 1998; given the high median redshift of objects in the FIRST survey ( $\bar{z} \sim 1$ ), the data obtained in the angular range  $0.3^\circ \leq \theta \leq 3^\circ$  provided by our analysis of the catalogue correspond to a range of spatial scales ( $r > 10h^{-1}\text{Mpc}$ ) where the linear regime still holds. As a check we calculated the integrated correlation function  $\bar{\xi}(r, z) \equiv \frac{3}{r^3} \int_0^r \xi(y, z) y^2 dy$  as obtained for  $\xi(r, z) = \xi(r)D^2(z)$  (growth of clustering under linear theory) in the case of  $\xi_{mass}(r)$  as described earlier in this section and  $b(z) = 1$ . This integral was performed at different red-

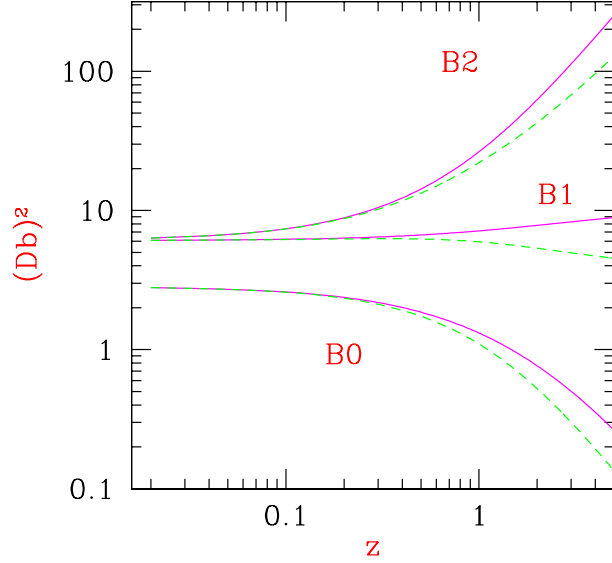


**Figure 5.** Trend of the quantity  $D(z)b(z)$  as a function of redshift for three different models of biasing as described in the text.  $\Omega_0$  is set to be 0.3, while  $b_0^{opt} = 1.46$ . The solid lines represent open models while the dashed lines are for flat models.

shifts and for  $\Omega = 1$  and the resulting integrated correlation functions have been compared with the expression

$$\bar{\xi} = \frac{x + 0.358x^3 + 0.0236x^6}{1 + 0.0134x^3 + 0.00202x^{9/2}} \quad x = a^2 \bar{\xi}_0(r_0) \quad (14)$$

from Hamilton et al., 1991 to take into account the effects of non-linear evolution. The results are shown in figure 4 where we plotted  $\bar{\xi}(r, z)$  as a function of the angular scale  $\theta = r/xa$  with  $x$  given by equation 4 in the case  $\Omega_0 = 1$ , for  $z = 0.1, 1, 2, 3, 4$ ; solid lines represent the evolution of the integrated correlation function under linear theory, while the dashed lines are obtained from equation (14). It is clear from the plot that differences between the two models occur only at angular scales significantly smaller than the range of our observations ( $0.3^\circ \leq \theta \leq 3^\circ$ ) which are bracketed by the two dashed vertical lines. This gives some confidence that our model assumptions are reasonable.

The biasing factor  $b(z)$  in equation (11) allows for evolution in the way radio sources trace the mass distribution. In principle  $b$  can be a function of both scale and redshift, but at  $z = 0$ , significant deviations from  $b(r) = const$  are seen only on small scales ( $r < 10h^{-1}\text{Mpc}$ ) (Bagla, 1997). Thus in the following analysis we ignore any variation of bias with scale. We take into consideration three possible models for the evolution of biasing as a function of the redshift (for an extensive study see Matarrese et al., 1997 and Moscardini et al., 1997). The first of these, called hereafter B0, is:

$$b(z) \equiv b_0 \simeq \frac{1}{\sigma_8^{mass}} \left( \frac{r_0}{5.4} \right)^{1.7/2}, \quad (15)$$

representing constant bias at all epochs. The two other models are derived from the expression

$$b(z) = b_{-1} + (b_0 - b_{-1})(1+z)^\beta \quad (16)$$

with

$$b_0 \simeq \frac{1}{\sigma_8^{mass}} \left( \frac{r_0}{5.4} \right)^{1.7/2}.$$

Setting  $b_{-1} = \beta = 1$  gives model B1, while setting  $b_{-1} = 0.41$ ,  $\beta \simeq 1.8$  gives model B2.

The B1 parameters have been chosen in agreement with the so-called *galaxy conserving model* (Fry, 1996; Tyson, 1988) in which galaxies form at some particular redshift and then evolve without losing their identity, by following the continuity equation. The latter set (B2) refers to results from N-body simulations (see e.g. Bagla, 1997) and describes the so-called *merging model* in which faint galaxies are subunits that merge to make up more luminous galaxies (Broadhurst et al., 1992; Clements & Couch, 1996; Baugh et al., 1996).  $r_0$  is the clustering length of radio sources at  $z = 0$  ( $\sim 10h^{-1}$  Mpc in our case, as measured by Peacock & Nicholson, 1991; see also Magliocchetti et al., 1998) while  $r_0^{gal} = 5.4h^{-1}$  Mpc is the corresponding value for optically-selected galaxies as measured in the APM survey, so that the factor  $\left(\frac{r_0}{5.4}\right)^{1.7/2}$  allows for the different bias level of 'optical' galaxies compared to radio objects as seen at zero redshift. The mass r.m.s. fluctuation amplitude inside a sphere of  $8h^{-1}$  Mpc is given by  $\sigma_8^{mass}$ , and the quantity  $b_0^{opt} = 1/\sigma_8^{mass}$  is the bias of the distribution of optical galaxies relative to the distribution of mass. This value depends on both the geometry and the normalisation of the power spectrum  $P(k)$ . Note that the amplitude of  $\xi_{mass}(r)$  in equation (11) depends on the evolution of the biasing factor with redshift given in equations (15-16) through the relation:

$$\xi_{radio}(r, 0) = b^2(0)\xi_{mass}(r). \quad (17)$$

From equation (17) we can therefore determine the values for the mass correlation length  $r_0^{mass}$  that turns out to be:

$$r_0^{mass} = 8 \left( \frac{(\sigma_8^{mass})^2}{c_\gamma} \right)^{1/\gamma}, \quad (18)$$

where  $c_\gamma$  is a factor depending on the slope of the correlation function at small scales (see Peebles, 1980).

As an illustration figure 5 shows the quantity  $D(z) b(z)$  as a function of redshift for the three biasing models described by equations (15-16) for  $\Omega_0 = 0.3$ , flat (dashed lines)/open (solid lines) Universe and  $b_0^{opt} = 1.46$ . The evolution of clustering with redshift/epoch is completely determined by the combination of bias  $b(z)$  and density growth rate  $D(z)$  (equation 11), and so the different forms of  $b(z)$ , give models where a) clustering decreasing with look-back time (B0), b) clustering roughly constant (B1) and c) clustering rapidly increasing with look-back time (B2).

To constrain an already wide parameter space we fix the value for the reduced Hubble constant as  $h_0 = 0.65$  (see e.g. Kundic et al., 1997). Moreover, it is almost impossible to discriminate between different values of  $\Omega_0$  through the evolution of clustering, because low density models in which clustering evolves slowly have a geometry which provides more time for evolution. This degeneracy in  $\Omega_0$  is often referred to as *cosmic conspiracy*. Hence we restrict our analysis to  $\Omega_0 = 0.4$ , allowing also for flat geometries ( $\Omega_0 + \Lambda = 1$ ). We adopt the normalisation of the r.m.s. mass fluctuations,  $\sigma_8^{mass}$ , determined from the 4-year COBE data by Bunn & White (1997). So choosing a well-defined cosmology (i.e. a

fixed value of  $\Omega_0$  and  $\Lambda$ ) fixes the value of  $\sigma_8$  and therefore the amplitude of  $\xi_{mass}(r)$ , given by  $r_0^{mass}$  from equation (18) Then the parameter  $b_0^{opt}$  in the expression for  $b(z)$  is also determined by equation (15) and (16). We then have:

$$\begin{aligned} \Omega_0 = 0.4 \quad \Lambda = 0 &\rightarrow \sigma_8^{mass} = 0.64; \quad r_0^{mass} = 3.31h^{-1} \text{Mpc} \\ \Omega_0 = 0.4 \quad \Lambda = 0.6 &\rightarrow \sigma_8^{mass} = 1.07; \quad r_0^{mass} = 6.23h^{-1} \text{Mpc} \end{aligned}$$

As a comparison for a standard CDM model we would have  $\sigma_8^{mass} = 1.22$ ;  $r_0^{mass} = 6.82h^{-1}$  Mpc. Thus it turns out that in  $\Lambda$ CDM and standard CDM (SCDM) models the distribution of optical galaxies is "antibiased" relative to the distribution of mass so that the amplitude of the corresponding  $\xi^{mass}(r)$  is higher than that found for galaxies; the opposite case pertains for open CDM (OCDM) models.

Concerning the constant bias case B0 we have instead decided to fix (ad hoc)  $\sigma_8^{mass} = 1$ , so that  $r_0^{mass} = 5.4 h^{-1}$  Mpc.

Note that in the case of  $\Gamma = 0.5$  both  $r_0^{mass}$  and  $\sigma_8^{mass}$  will differ from the values expressed for  $\Gamma = 0.2$ . In more detail we have:

$$\begin{aligned} \Omega_0 = 0.4 \quad \Lambda = 0 &\rightarrow \sigma_8^{mass} = 1.51; \quad r_0^{mass} = 8.95h^{-1} \text{Mpc} \\ \Omega_0 = 0.4 \quad \Lambda = 0.6 &\rightarrow \sigma_8^{mass} = 2.52; \quad r_0^{mass} = 15.8h^{-1} \text{Mpc}, \end{aligned}$$

i.e. if  $\Gamma = 0.5$ , in both the  $\Lambda$ CDM and OCDM models the distribution of galaxies is "antibiased" relative to the distribution of mass.

## 4 PREDICTIONS FOR $W(\theta)$

In this section we will focus our attention on the predicted angular correlation function  $w(\theta)$  obtained for two different CDM models with respectively,  $\Gamma = 0.5$  (standard CDM model) and  $\Gamma = 0.2$  (modified CDM model), values that bracket the range of models providing the best fit to the present observations of the power spectrum  $P(k)$  (Peacock & Dodds, 1994). Note that these models treat  $\Gamma$  as a free parameter independent of  $h_0\Omega_0$ , and so do not represent consistent CDM models.

We will focus on the three different redshift distributions of radio sources (N1, N2, N3) described in section 2, and on the three functional forms for the evolution of the biasing with redshift (B0, B1, B2) introduced in section 3. In order to test the self-consistency of the predictions of each model, we consider two different flux-cuts: 3mJy, the lowest flux limit where the incompleteness of the survey is negligible (see Magliocchetti et al., 1998) - and 10mJy, the brightest flux limit for which the measurements of  $w_{obs}(\theta)$  are not dominated by the errors). In what follows we always start by considering models derived for  $F > 10$ mJy, because the differences between the different  $N(z)$ 's are less significant than for fainter fluxes (see figures 1 and 2). In particular the relative weight of the low-redshift component and of the  $z \sim 1$  bump are much less variable at higher flux limits.

We will first show the results for a CDM power spectrum with  $\Gamma = 0.2$  and then compare them to those with  $\Gamma = 0.5$ . The theoretical estimates of  $w(\theta)$  obtained at 10mJy are to be compared with those for 3mJy, while keeping all the

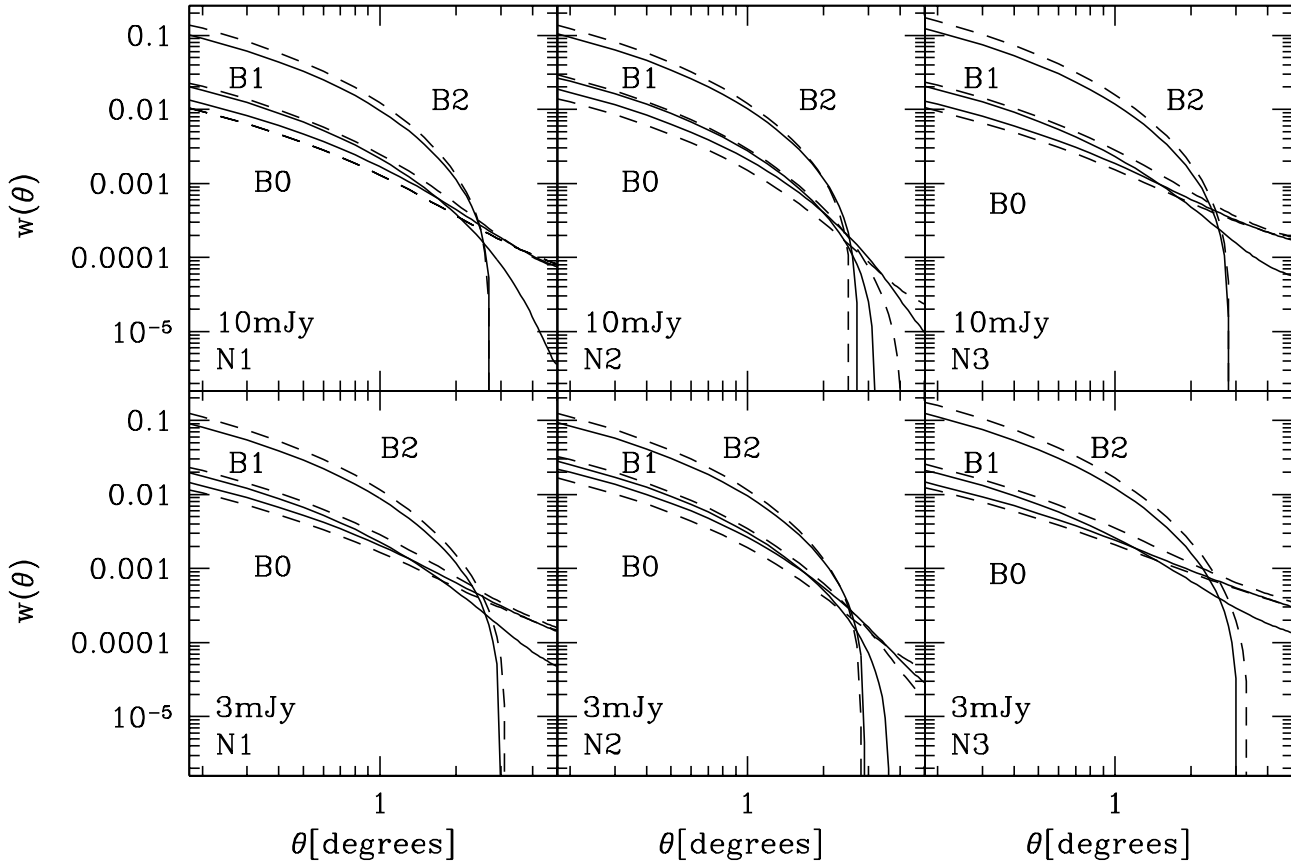


**Figure 6.** Theoretical prediction of the angular correlation function for  $\Gamma = 0.2$ ,  $N(z) \equiv N1, N2, N3$  at 10mJy and 3mJy, and different bias models as described in the text. The solid lines are for open models while the dashed lines indicate spatially-flat models.

other parameters fixed, in order to test the consistency of the predictions of different models for  $N(z)$ .

In Figure 6 we plot the theoretical estimates of  $w(\theta)$  (in the case  $\Gamma = 0.2$ ) at 10mJy (upper panel) and 3mJy (lower panel), for the three models of  $N(z)$  introduced in section 2 and the three models for the evolution of bias with redshift of section 3. The correlation length  $r_0$  in equations 15 and 16 has been fixed at  $10h^{-1}$  Mpc in agreement with both our previous estimate (Magliocchetti et al., 1998) and the results found by Peacock and Nicholson (1991). The solid lines are for open ( $\Omega = 0.4$ ) models while the dashed lines are for flat ( $\Lambda \neq 0$ ) geometries.

Independent of the flux cut, the discrimination amongst different models comes both from the eventual fall of  $w(\theta)$  at large angular scales and from its overall amplitude. The overall amplitude of the angular correlation function is mainly related to the level of bias at high  $z$ : models char-

acterised by a bias factor increasing with redshift (B1/B2) show a stronger clustering signal, especially at smaller angular scales, relative to models with constant bias (B0). Their amplitude increases as the dependence of  $b(z)$  on the factor  $(1+z)$  in equation (16) becomes steeper, as can be seen by comparing the B2 with the B1 models. The difference in amplitude between the B0 and B1 models is not pronounced; this effect is primarily due to the lower normalisation of the B1 models deriving from having taken  $\sigma_8^{mass} \neq 1$  as opposed to the assumption of  $\sigma_8^{mass} = 1$  in the B0 case. Furthermore, as the main contribution to the clustering signal at large angular scales is given by low-redshift objects (see Cress & Kamionkowski, 1998), the factor  $(1+z)$  is not strong enough to drive the evolution of the B1 models far from that described by B0.

The fall at large angular scales depends instead on the negative feature in  $\xi$ , a genuine feature of CDM-like models, as well as on the amplitude of the low- $z$  component in the  $N(z)$ . Note that in equations 6 and 9 the integral is weighted

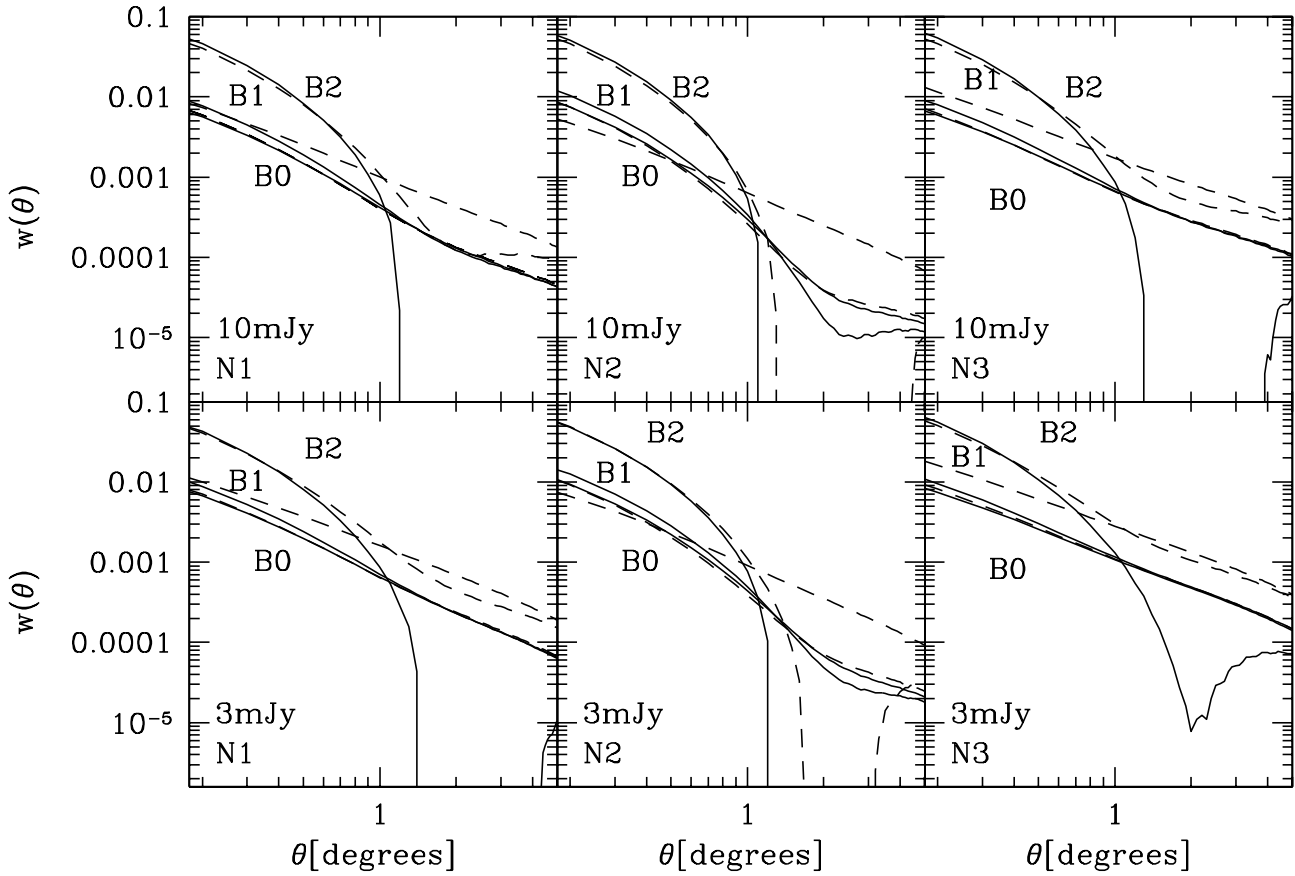


**Figure 7.** Theoretical prediction of the angular correlation function for  $\Gamma = 0.5$ ,  $N(z) \equiv N1, N2, N3$  at 10mJy and 3mJy, and different bias models as shown in the figure. The solid lines are for open models while the dashed lines indicate spatially flat-models.

by  $N(z)^2$ , so the spike makes a significant contribution to  $w(\theta)$  even though the volume is small. The low- $z$  amplitude describes the relative contribution of the local population of radio objects, that, as already mentioned, is the component which provides the dominant contribution to the clustering signal at large angular scales (Cress & Kamionkowsky, 1998). In fact from figure 6 one can see how all the correlation functions obtained for N2 (no low-redshift component) drop at  $\theta \sim 2^\circ$ , while those for N3 and N1 models, characterised by a larger low-redshift component, flatten out at this angular scale, with a positive tail at larger scales that becomes more predominant as the number of nearby objects is increased. This effect is stronger at 3mJy than at 10mJy because the amplitude of the local population of star-bursting galaxies increases as the flux threshold is lowered.

The predictions for  $w(\theta)$  for the case of  $\Gamma = 0.5$  are illustrated in figure 7; the models show basically the same features as those obtained in the analysis for  $\Gamma = 0.2$ , indicating

very little dependence on the value of the shape parameter  $\Gamma$ .

## 5 RESULTS FROM THE COUNTS IN CELLS ANALYSIS AT DIFFERENT FLUX LIMITS

This section considers the counts-in-cells analysis of the FIRST catalogue carried out at different flux limits; we then compare the predictions with the corresponding measurements in section 6. We measured the clustering of radio objects using the so-called *galaxy distribution function* that gives the probability of finding  $N$  objects in a cell of particular size and shape. By defining the  $k$ -th moment of the counts as

$$\mu_k = \langle (N - \bar{N})^k \rangle \quad (19)$$

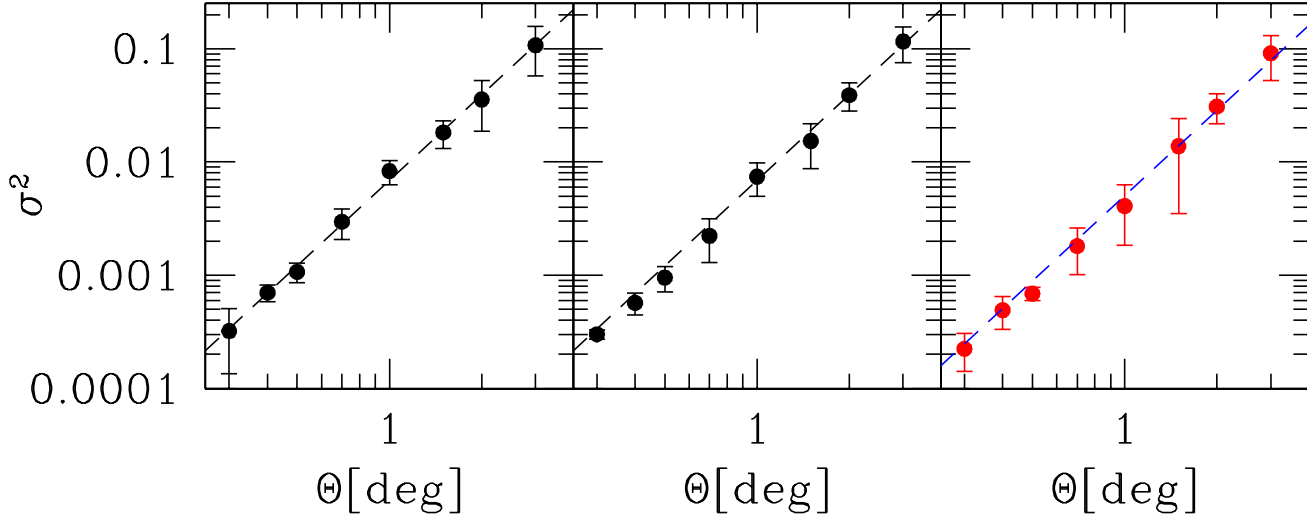


**Figure 8.** The normalised variance  $\sigma^2$  vs the cell size  $\Theta$  for the FIRST survey for objects brighter than 5mJy (left panel), 7mJy (middle panel) and 10mJy (right panel). Errors are estimated from the variance in four random subsets.

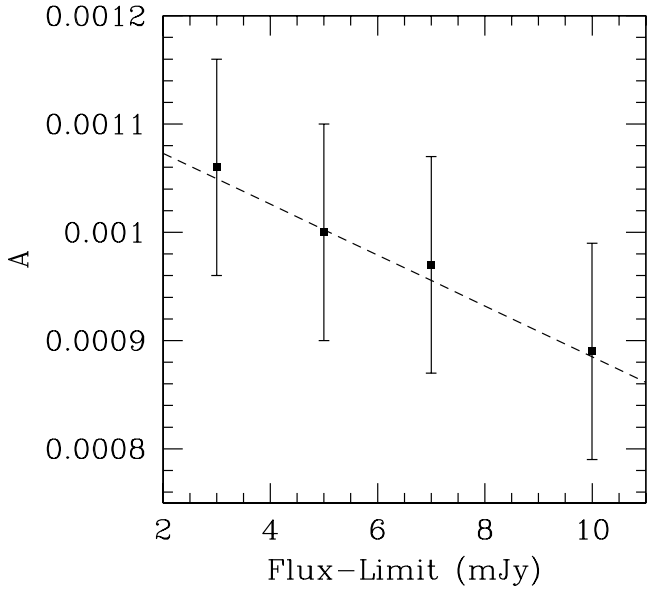


**Figure 9.** Amplitude of the angular correlation function  $w_{obs}(\theta)$  as measured from the FIRST survey as a function of the flux limit.

where  $\bar{N} = n\Omega$  is the mean count in the solid angle  $\Omega$ , we have that the second moment  $\mu_2$  of the galaxy distribution function is related to the two-point correlation function  $w_{12}$  through the expression

$$\mu_2 = \bar{N} + (\bar{N})^2 \Psi_2 \quad (20)$$

where  $\bar{N}$  is the shot noise resulting from the discrete nature of the sources (Poisson noise), and

$$\Psi_2 \equiv \frac{1}{\Omega^2} \int w_{12} d\Omega_1 d\Omega_2 \quad (21)$$

is the normalised variance in terms of the two-point correlation function integrated over a cell of area  $\Omega$  and particular shape. By assuming a power-law form

$$w(\theta) = A \theta^{1-\gamma}, \quad (22)$$

and by considering square cells of size  $\Omega = \Theta \times \Theta$  square degrees, we can evaluate the integral in equation (21) (see Totsuji & Kihara, 1969), obtaining

$$\sigma^2 \equiv \frac{\mu_2 - \bar{N}}{(\bar{N}/\Omega)^2} = \int A \theta^{1-\gamma} d\Omega_1 d\Omega_2 = A C_\gamma \Theta^{5-\gamma} \quad (23)$$

where  $C_\gamma(\gamma)$  is a coefficient which can be evaluated numerically by Monte Carlo methods (Lahav & Saslaw, 1992). It is therefore possible to use the  $\sigma^2 - \Theta$  relation to evaluate the two parameters ( $A, \gamma$ ) which describe the correlation function (22).

The following analysis has been carried out as in Magliocchetti et al. (1998) for different versions of the original FIRST catalogue obtained by combining source components into single source, following well defined criteria. The results are shown in figure 8 where we plot  $\sigma^2$  as a function of  $\Theta$  for different flux limits. The slopes and the intercepts of the plots are estimated by a least-squares procedure minimising



the quantity

$$\chi^2(a, b) = \sum_{i=1}^N \left( \frac{\log(\sigma)_i - a - b \log(\Theta)_i}{\Delta_i} \right)^2 \quad (24)$$

with  $b \equiv (5 - \gamma)$ ,  $a \equiv \log(AC_\gamma)$ . The errors  $\Delta_i$  are obtained using the ‘partition bootstrap method’ in which the normalised variance is calculated for four subdivisions of the survey region and the standard deviation of these measurements at each angle is used as a measure of the error. From this analysis we find, for  $F \geq 3\text{mJy}$ ,  $F \geq 5\text{mJy}$ ,  $F \geq 7\text{mJy}$  and  $F \geq 10\text{mJy}$  respectively:

$$\gamma = 2.50 \pm 0.1 \quad ; \quad A = (1.06 \pm 0.1) \cdot 10^{-3}, \quad (25)$$

$$\gamma = 2.50 \pm 0.1 \quad ; \quad A = (1.00 \pm 0.1) \cdot 10^{-3}, \quad (26)$$

$$\gamma = 2.50 \pm 0.09 \quad ; \quad A = (0.97 \pm 0.1) \cdot 10^{-3}, \quad (27)$$

$$\gamma = 2.40 \pm 0.2 \quad ; \quad A = (0.89 \pm 0.1) \cdot 10^{-3}, \quad (28)$$

The 3mJy measurement is taken from Magliocchetti et al. (1998). Above 10mJy the measurements are dominated by Poisson errors.

From equations (26), (27) and (28) we have that the slope  $\gamma$  of the correlation function (see eq. 22) is independent of the flux limit in the range  $3\text{mJy} \leq F \leq 10\text{mJy}$  (see Magliocchetti et al., 1998 for the results at 3mJy). Furthermore we find that the amplitudes  $A$  at each flux-cut are vary smoothly with the flux limit, as shown in figure 9. We can therefore be confident that the clustering signal found in our analysis is mainly given by populations of radio objects which do not change their clustering properties as the flux level cut is increased. This result will be of particular help in the next sections when we compare the theoretical predictions for the correlation function with measurements at different flux limits.

## 6 COMPARISONS WITH THE DATA

One of the main reasons for preferring the variance statistic (i.e. the counts in cells analysis) to the the direct evaluation of the correlation function  $\xi_{radio}$  is that  $\sigma^2$  is a cumulative quantity which provides a complete description of large-scale structure in a more robust way. Therefore, in order to match the models obtained for the angular correlation function in section 4 with the results inferred from the counts in cells analysis, one has to integrate  $w(\theta)$  to get the predictions for the variance of the distribution of sources. This can be done by means of equation (23) which, for a generic  $w(\theta)$ , is written as

$$\sigma^2 = \int w(\theta) \delta\Omega_1 \delta\Omega_2, \quad (29)$$

and in the case of square cells, can be expressed as the two dimensional integral

$$\sigma^2(\Theta) = \Theta^2 \int_0^\Theta dx \int_0^\Theta w(\theta) dy, \quad (30)$$

where  $\Theta^2$  is the area of the cells and  $\theta = \sqrt{x^2 + y^2}$ . The quantity given by equation (29) has then been evaluated

for all the  $w(\theta)$  models illustrated in section 4 and the corresponding  $\sigma^2$ 's have been compared with the estimates of  $\sigma_{obs}^2$  obtained from the data both at 3mJy and 10mJy as explained in section 5 and in Magliocchetti et al. (1998).

Figures 10 and 11 show the results for  $\Gamma = 0.2$  and  $\Gamma = 0.5$  respectively; the symbols are as in section 4 and once again the solid lines are for open models while the dashed lines are for spatially-flat models. Independent of the functional form adopted for the redshift distribution  $N(z)$  and of the flux cut, models with bias strongly evolving with redshift can be ruled by the data with a high confidence level ( $\gtrsim 3\sigma$ ) as they grossly overestimate the amplitude of  $\sigma^2(\Theta)$  at all scales. Although the predictions for constant bias (B0) provide a somewhat better fit to the data (particularly for  $\Gamma = 0.2$ ), the B0 (constant bias) and the B1 (bias linearly evolving with redshift) models are almost degenerate with reference to the measurements. As already mentioned in section 4, this effect is due to the low normalisation of the mass correlation function  $\xi_{mass}(r)$  in the B1 case, resulting from the assumption that optical galaxies are biased relative to the distribution of mass, and from the fact that for B1 (contrary to the B2 models) the dependence of  $b(z)$  on the redshift is not strong enough to drive the evolution of  $\xi_{radio}(r, z)$  to higher amplitudes, on these angular scales.

If one assumes that radio sources are indeed strongly biased with respect to ‘‘normal’’ galaxies by the factor  $(10/5.4)^{1.7}$  appearing in equations (15) and (16), then the conclusion of the B0 model as favoured for the interpretation of the data is in agreement with the results found by Matarrese et al. (1997) and Frieman & Gaztañaga (1994) from the angular correlation function in optical/infrared surveys.

This kind of analysis apparently is not sensitive to differences in  $N(z)$ 's. As  $\sigma^2$  is an integral quantity, its behaviour has very little dependence on the form of the tail of  $w(\theta)$  at large angular scales where the clustering signal is weaker by at least two orders of magnitude than that at  $\theta \sim 0.1^\circ$ . Thus, although the models for  $w(\theta)$  for different redshift distributions show remarkable differences, the combined effects of the integral (28) and the presence of observational uncertainties in the estimates of  $\sigma_{obs}^2(\Theta)$  wash out these differences.

## 7 THE CLUSTERING EVOLUTION FOR DIFFERENT RADIO POPULATIONS

A major problem in the analysis and interpretation of the clustering of radio sources at faint flux limits is the mixing of different populations. The brighter objects in a deep radio survey are identified with powerful radio-loud QSOs and AGN's; the fainter objects ( $\lesssim 3\text{mJy}$ ) are dominated by a population of faint low- $z$  sources which are local starbursting galaxies (see Wall, 1994). As radio-loud QSOs tend to be hosted by giant ellipticals within rich clusters (see e.g. Cristiani, 1998), these objects show a much stronger correlation than normal field spirals (see also Loveday et al., 1995) containing the population of star-bursting galaxies. It is therefore of crucial importance to take into account the characteristics of these two different populations to get information on their clustering properties and on the evo-

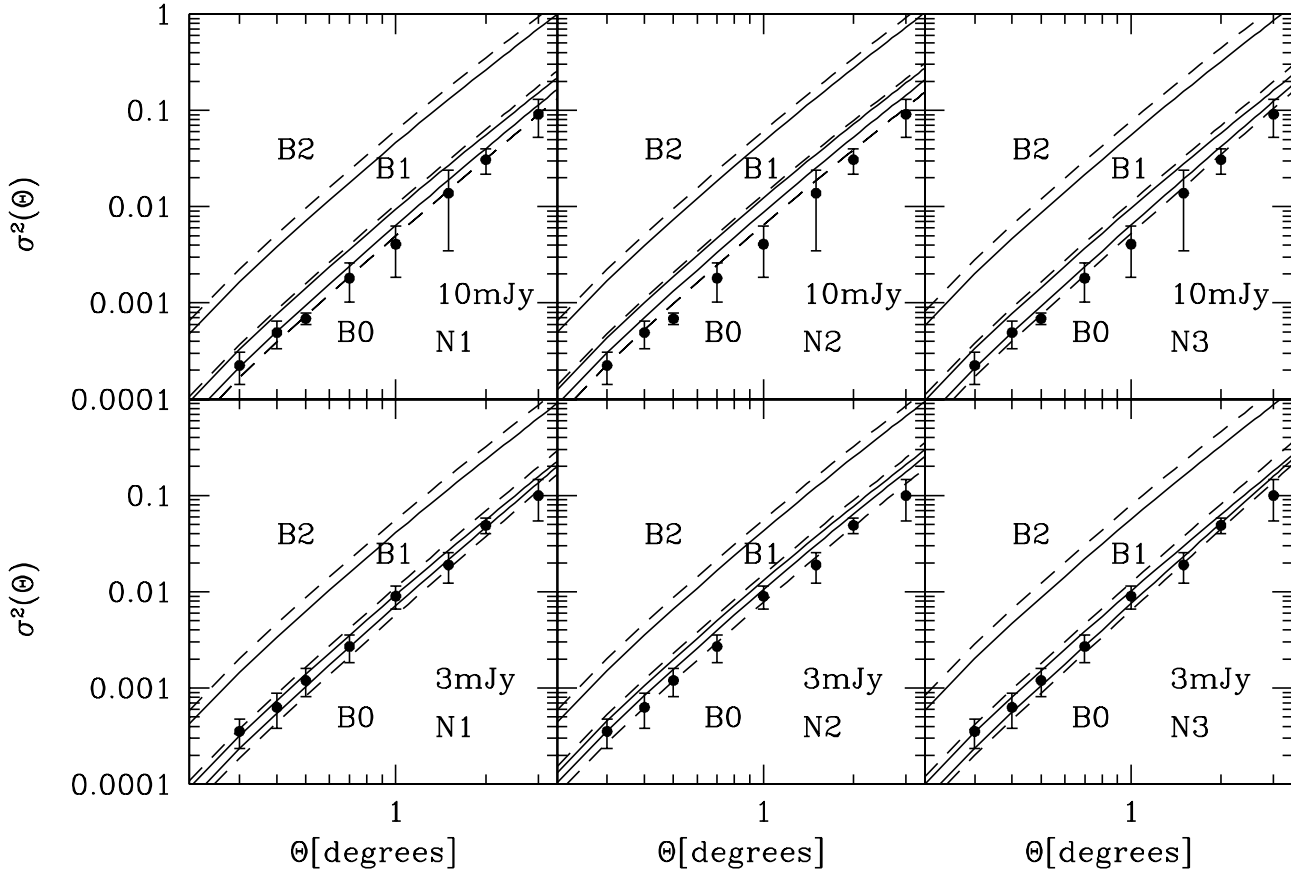


**Figure 10.** Theoretical predictions for the normalised variance  $\sigma^2$  in the case of  $\Gamma = 0.2$ ,  $N(z) \equiv N1, N2, N3$  at 10mJy and 3mJy, and different bias models. The solid lines are for open models while the dashed lines are for spatially-flat models. The data are from the FIRST survey.

lution of bias with redshift. Theoretical works suggest that bias depends on the mass of the dark matter halos in which galaxies were born (Mo & White, 1996) and therefore its dependence can also be related to the mass of the galaxy itself in the hypothesis that the most “visible” galaxies reside within the most massive dark matter halos.

To perform our analysis we use a simple approach assuming at low redshifts the clustering signal is dominated by the starbursting objects while at higher  $z$ 's both the populations contribute. This approximation is justified by the observational evidence of a drastic drop in the number of quasars in the nearby universe. We therefore write the correlation function as follows:

$$\xi_{tot}(r, z) = [A^2\xi_A + 2AB(\xi_A\xi_B)^{1/2} + B^2\xi_B] \quad (31)$$

where  $\xi_A(r, z)$  is the correlation function for the starbursting galaxies,  $\xi_B(r, z)$  is for radio-loud quasars, and  $A$  and  $B$  are the relative space densities the two populations normalized so that  $A + B = 1$ . We assume that  $B = 0$  for  $z < 0.1$ , and consider three possibilities for  $z > 0.1$ : starburst dominated,

$A = 0.8, B = 0.2$ ; an equal mix  $A = 0.5, B = 0.5$ ; and AGN dominated,  $A = 0.2, B = 0.8$ . For the starburst correlation function we use  $\xi_A(r, z) = \xi D(z)^2 b'(z)^2$ , where  $\xi(r)$  and  $D(z)$  are as expressed in section 3. For the AGN correlation function we use  $\xi_B(r, z) = \xi' D(z)^2 b(z)^2$  where  $\xi'(r)$  is the effective linear bias mass correlation function for QSOs: we assume on large scales that it is the linear prediction for a CDM model with generic  $\Gamma$ , while at small scales  $\xi$  has been extrapolated as a power-law of slope  $-2.1$  as found from the analysis of the clustering of bright-early type galaxies in the Stromlo-APM redshift survey (Loveday et al., 1995). Note that the value of 2.1 for the slope is different from that used in section 3, where we considered the radio sample to be homogeneous.  $b(z)$  and  $b'(z)$  are the bias associated with bright radio sources (QSOs + AGN) and spiral galaxies (starbursting population) relative to the distribution of mass; their expressions are given by equations (15) and (16) assuming  $r_0 \sim 10h^{-1}\text{Mpc}$  (powerful radio sources) and  $r_0 \sim 5.4h^{-1}\text{Mpc}$  (optical-galaxies). This yields for example, in the case of constant bias (B0) models, that the

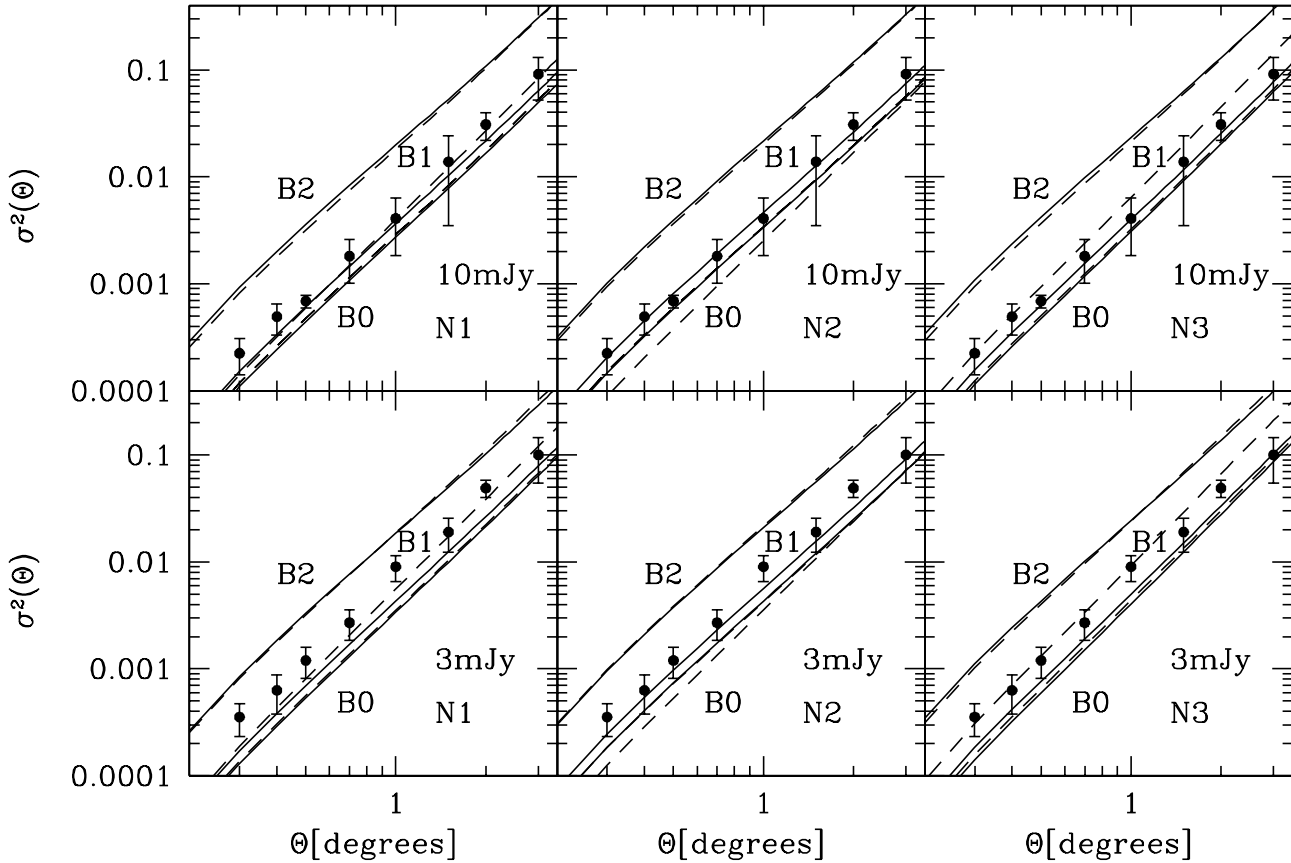


**Figure 11.** Theoretical predictions for the normalised variance  $\sigma^2$  in the case of  $\Gamma = 0.5$ ,  $N(z) \equiv N1, N2, N3$  at 10mJy and 3mJy, and different bias models. The solid lines are for open models while the dashed lines are for spatially-flat models. The data are from the FIRST survey.

starbursting population is indeed unbiased ( $b(z) = 1$ ), while the AGN population shows a higher bias relative to the distribution of the mass; at  $z = 0$ ,  $b(0) = \left(\frac{10}{5.4}\right)^{2.1/2} \frac{1}{\sigma_{mass}^8}$ . The expression for  $\xi_{tot}(r, z)$  has then been projected by means of the Limber equation (1) in order to get the relative functional form for the angular correlation function  $w(\theta)$ .

As Cress and Kamionkowsky (1998) have indicated, at scales  $\theta \gtrsim 1^\circ$  the angular correlation function is dominated by nearby objects (within  $z \lesssim 0.1$ ), while at scales  $\theta \sim 0.1^\circ$  there is an equal contribution from local ( $z \lesssim 0.1$ ) and distant ( $z \gtrsim 0.1$ ) sources. Thus, to study the evolution of the clustering of bright distant objects we have to compare our models of  $w(\theta)$  with the observed correlation function pushing the measurements down to angles  $\theta \sim 0.02^\circ$ . Note that, as can be seen in figure 4, the assumption of growth of clustering under linear theory is still a good approximation at

these angular scales. The counts-in-cells statistics for the FIRST survey are dominated by shot (Poisson) noise for  $\theta \lesssim 0.3^\circ$  (see Magliocchetti et al., 1998) and so to extend the range of measurement down to smaller scales we have measured angular correlation function  $w_{obs}(\theta)$  directly from the catalogue.

We recall here that the angular correlation function  $w_{12} = w(\theta)$  gives the excess of probability, with respect to a Poisson random distribution, of finding two sources in the solid angles  $\delta\Omega_1$   $\delta\Omega_2$  separated by an angle  $\theta$ , and it is defined as

$$\delta P = n^2 \delta\Omega_1 \delta\Omega_2 [1 + w(\theta)] \quad (32)$$

where  $n$  is the mean number density of objects in the catalogue under consideration. We measured  $w_{obs}$  from the estimator (Hamilton, 1993)

$$w_{obs}(\theta) = 4 \frac{DD}{DR^2} \frac{RR}{DR^2} - 1 \quad (33)$$

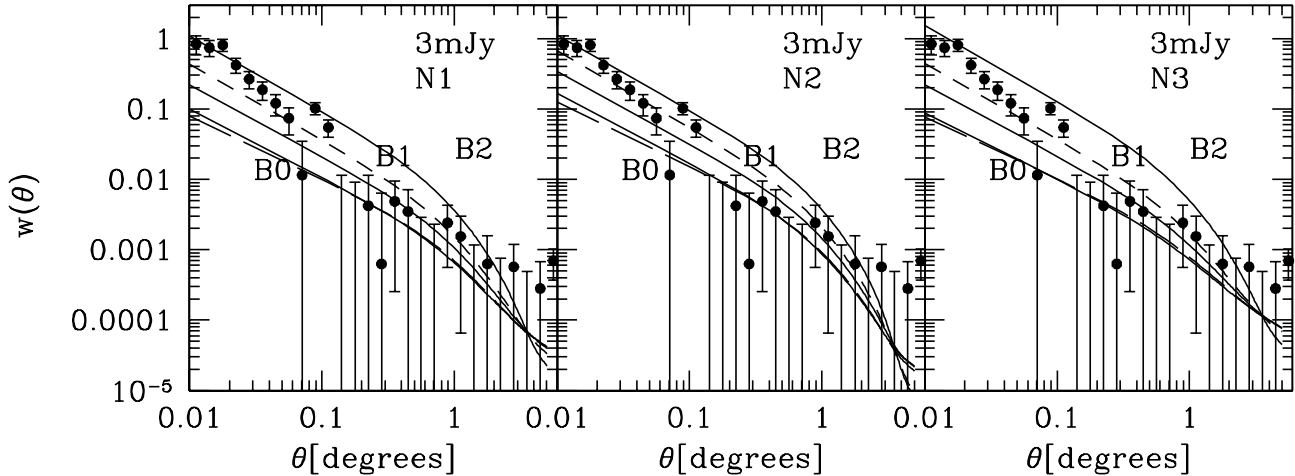


**Figure 12.** Theoretical prediction for the angular correlation function in the case of  $\Gamma = 0.2$ ,  $N(z) \equiv N1, N2, N3$  at 3mJy, and different bias models as shown in the figure. The solid lines are for models with  $A = B = 0.5$ , the long-dashed lines are for  $A = 0.8$ ,  $B = 0.2$ , while the short-dashed lines stand for  $A = 0.2$  and  $B = 0.8$  (see text for details). The data are obtained from measurements of  $w_{obs}(\theta)$  using equation 33. The error bars show the Poisson estimates for the catalogue under consideration.

where  $DD$  is the number of distinct data-data pairs,  $DR$  is the number of random-data pairs and  $RR$  is the number of random-random pairs as a function of angular separation and where the random data have been obtained by generating a random catalogue of positions and selected sources above the sensitivity limit from the coverage map (see Magliocchetti et al., 1998 for further information about the catalogue).

Given the very weak dependence of the angular correlation function on geometry, the shape parameter of the power spectrum  $\Gamma$  and the flux cut (at least for  $F \leq 10\text{mJy}$ ), we restrict our analysis to  $\Omega = 1$ ,  $\Gamma = 0.2$  and  $F \geq 3\text{mJy}$ , while still allowing for different functional forms of the redshift distribution  $N(z)$ . All the models assume that the distribution of starburst objects is unbiased with respect to the mass distribution, justified by the results obtained for the more local population in section 6. The corresponding models are shown in figure 12 where we also plot  $w_{obs}$  taken from the FIRST survey at 3mJy; the error bars show Poisson estimates for the catalogue under consideration. The solid lines are for models in which the distribution of the AGN population is unbiased (B0), has a bias linearly evolving with redshift (B1) and has a bias strongly evolving with  $z$  (B2). The predictions have been calculated in the case of the two populations equally contributing to the clustering signal ( $A = B = 0.5$ ). As figure 12 shows, while at large angular scales the B0 and B1 models are roughly degenerate as in section 6, pushing the analysis down to smaller scales removes this degeneracy. In fact the B0 and B2 mod-

els are ruled out as possible descriptions of the data as they show either too small (B0) or too large (B2) amplitude, especially at intermediate scales. The best fit is provided by the B1 curves i.e. by models in which the distribution of the starbursting population is taken to be roughly unbiased while that one for the AGN population shows a bias linearly evolving with redshift.

The effect of varying the relative weight of the two populations in the B1 model is shown in figure 12 for the two cases:  $\sim 20\%$  starburst and  $\sim 80\%$  AGN (short dashed lines) and  $\sim 80\%$  starburst and  $\sim 20\%$  AGN (long dashed lines). The agreement with the data is best for the AGN dominated model. The notable differences for different  $N(z)$ 's found in section 4 reside primarily in the part of the angular correlation function at large scales where the signal is dominated by the noise.

The fact that we need a biased distribution of AGN in order to match the data is in agreement with the hierarchical models of galaxy formation predicting the less massive objects to be less strongly clustered than those formed in the higher and biased peaks of the density field (Giavalisco et al., 1998), with the most powerful sources being hosted by the most massive dark matter halos, and the biasing factor depending (at least) both on the epoch and the type of objects under consideration (i.e. on the halo mass).

## 8 CONCLUSIONS

To put constraints on the redshift distribution  $N(z)$  of radio objects at faint fluxes and on their clustering and biasing properties, we have calculated predictions for the angular correlation function  $w(\theta)$  using three models for  $N(z)$  and three models for the clustering evolution. The three models for the redshift distribution have been chosen to span the range of reasonable possibilities. The predictions for  $w(\theta)$  have been calculated for a  $\xi_{mass}$  obtained from two CDM models ( $\Gamma = 0.2$  and  $\Gamma = 0.5$ ), three different assumptions for the evolution of the bias and in the case  $\Omega_0 = 0.4$ , both flat and open space. We chose a fixed value for the density parameter because of the degeneracy amongst predictions obtained for different  $\Omega_0$ 's. The bias models correspond to three sensible galaxy evolution models (galaxies tracing the mass at all epochs - constant bias;  $b(z) \propto (1+z)$  - galaxy conserving model;  $b(z) \propto (1+z)^{1.8}$  - galaxy merging model).

The discrimination amongst different models comes both from the fall of the calculated  $w(\theta)$  at large angular scales and from its overall amplitude. The fall depends on the negative feature in  $\xi$  at large scales, which is a generic feature of CDM-like models, and also on the low- $z$  component in the  $N(z)$  whose amplitude depends on the presence and relative contribution of any local population of radio objects. The overall amplitude of the angular correlation function is instead mainly related to the level of bias at high redshift.

For a comparison with the data inferred from the counts-in-cells analysis of the FIRST survey we integrated the models for  $w(\theta)$  to calculate the corresponding predictions for the variance of the distribution  $\sigma^2$ ; we then matched the results with the measurements for different flux limits presented in section 1 and in Magliocchetti et al. (1998). Although models for the angular correlation function obtained for different  $N(z)$  show quite remarkable differences, in the framework of this analysis it is not possible to discriminate amongst them, given the errors in the measurements and the fact that the integral used to calculate  $\sigma^2$  washes out the differences.

Concerning the bias evolution, all the models of bias strongly dependent on redshift can be ruled out with high confidence level as they grossly overestimate the amplitude of  $\sigma^2$  at all scales. There is a degeneracy between models with constant bias and those for bias depending linearly on redshift, although the predictions for constant bias are mildly preferred by the data, especially for  $\Gamma = 0.2$ . The analysis is quite insensitive to the geometry of the Universe.

As a further step, we introduced a model for the correlation function able to account for a mixing of populations with completely different properties, the first population of faint starbursting/spiral galaxies, the second one of AGN-powered objects normally hosted by bright ellipticals. We assumed that starbursting population traces the distribution of mass at all times, and we allowed for biasing evolution in the case of radio-loud AGN. Appropriate measurements for  $w_{obs}(\theta)$  were made directly from the catalogue. It turns out that an evolution of bias with redshift is required for AGN to match the data. The model that best fits the observed angular correlation function is given by the sum of a) a less numerous population of faint starbursting

sources, with clustering properties very similar to normal spiral galaxies and a distribution that is roughly unbiased relative to the distribution of mass, and b) a more numerous population of radio-loud AGN's much more strongly clustered and whose distribution is biased relative to the distribution of the mass, with a bias factor which evolves linearly with redshift. This result is in good agreement with hierarchical CDM theories of galaxy formation that predict the lower luminosity/lower mass objects being less clustered than the high-luminosity sources, with the brighter sources being associated with higher (and biased) peaks in the dark matter distribution.

There are crucial observations needed to further the analysis: in particular observational measurements of  $N(z)$ , from identifications and redshift measurements for a complete sample, would be of great importance in constraining structure formation models as well as understanding the distribution and evolution with time of the different populations of radio objects at mJy levels.

## ACKNOWLEDGEMENTS

MM acknowledges support from the Isaac Newton Scholarship. We thank George Efstathiou, Jarle Brinchmann and Jasjeet Bagla for helpful discussion.

## REFERENCES

- Bagla, J.S., 1997; astro-ph/9711081  
 Baugh C.M., Cole S., Frenk C.S., 1996; *MNRAS*, **282**, L27  
 Bond J.R., Efstathiou G., 1984; *ApJ*, **285**, L45  
 Becker R.H., White R.L., Helfand D.J., 1995; *ApJ*, **450**, 559  
 Broadhurst T.J., Ellis R.S., Glazebrook K., 1992; *Nat*, **355**, 55  
 Bunn E.F., White M., 1997; *ApJ*, **480**, 6  
 Clements D.L., Couch W.J., 1996; *MNRAS*, **280**, L43  
 Cress C.M., Helfand D.J., Becker R.H., Gregg M.D., White R.L., 1996; *ApJ*, **473**, 7  
 Cress C.M., Kamionkowski M., 1998; astro-ph/9801284  
 Cristiani S., 1998; 1998elss.confE..41C  
 Dunlop J.S., Peacock J.A., 1990; *MNRAS*, **247**, 19  
 Frieman J.A., Gaztañaga E., 1994; *ApJ*, **425**, 392  
 Fry J.N. 1996; *ApJ*, **461**, L65  
 Giavalisco M. et al. 1998b; in preparation  
 Hamilton A.J.S., 1993; *ApJ*, **417**, 19  
 Hamilton A.J.S., Kumar P., Lu E., Matthews A. 1991; *ApJ*, **374**, L1  
 Kooiman L.K., Burns J.O., Klypin A.A., 1995; *ApJ*, **448**, 500  
 Kundic T., Turner E.L., Colley W.N., Gott J.R.III, Rhoads J.E., Wang Y., Bergeron L.E., Gloria K.A., Long D.C., Malhotra S., Wambsgans J., 1997; *ApJ*, **482**, 75  
 Lahav O., Lilje P.B., Primack J.R., Rees M.J., 1991; *MNRAS*, **251**, 128  
 Lahav O., Saslaw W.C., 1992; *ApJ*, **396**, 430  
 Loan A.J., Wall J.V., Lahav O., 1997; *MNRAS*, **286**, 994  
 Loveday J., Maddox S.J., Efstathiou G., Peterson B.A.; 1995 *ApJ*, **442**, 457  
 Maddox S.J., Efstathiou G., Sutherland W.J., Loveday J., 1990; *MNRAS*, **242**, 43P  
 Magliocchetti M., Maddox S.J., Lahav O., Wall J.V., 1998; astro-ph/9802269  
 Matarrese S., Coles P., Lucchin F., Moscardini L., 1997; *MNRAS*, **286**, 115  
 Mo H.J., White S.D.M., 1996; *MNRAS*, **282**, 347

- Moscardini L., Coles P., Lucchin F., Matarrese S., 1997; astro-ph/9712184
- Peacock J.A., Nicholson D., 1991; *MNRAS*, **253**, 307
- Peacock J.A., Dodds S.J. 1994; *MNRAS*, **267**, 1020
- Peacock J.A., 1997; *MNRAS*, **284**, 885
- Peebles P.J.E., 1980; *The Large-Scale Structure of the Universe*, Princeton University Press
- Peebles P.J.E., 1984; *ApJ*, **284**, 439
- Seldner M., Peebles P.J.E., 1981; *MNRAS*, **194**, 251
- Shaver P.A., Pierre M., 1989; *A&A*, **220**, 35
- Sicotte H., 1995; *PhD thesis*, Princeton University
- Steidel C.C., Giavalisco M., Pettini M., Dickinson M., Adelberger K.L., 1996; *ApJ*, **462**, L17
- Steidel C.C., Adelberger K.L., Dickinson M., Giavalisco M., Pettini M., Kellog M., 1997; astro-ph/9708125
- Steidel C.C., Adelberger K.L., Giavalisco M., Dickinson M., Pettini M., Kellog M., 1998; astro-ph/9805267
- Tegmark M., Peebles P.J.E., 1998; astro-ph/980407
- Totsuji H., Kihara T., 1969; *PASJ*, **21**, 221
- Treyer M.A., Lahav O. 1996; *MNRAS*, **280**, 469
- Tyson J.A., 1988; *AJ*, **91**, 1
- Wall J.V., 1994; *Austr. J. Phys.*, **47**, 625
- Wall J.V., Jackson C.A., 1997; *MNRAS*, **290** L17
- Windhorst R.A., Miley G.K., Owen F.N., Kron R.G., Koo R.C., 1985; *ApJ*, **289**, 494